

# Lawrence Berkeley National Laboratory

## Recent Work

### Title

A MODEL FOR THE ANODIC DISSOLUTION OF IRON IN SULFURIC ACID

### Permalink

<https://escholarship.org/uc/item/8sb32190>

### Author

Law, C.G.

### Publication Date

1979-05-01

Submitted to the Journal of the Electrochemistry  
Society

LBL-8508  
Preprint

A MODEL FOR THE ANODIC DISSOLUTION OF IRON  
IN SULFURIC ACID

Clarence G. Law, Jr. and John Newman

May 1979

RECEIVED  
BERKELEY LABORATORY

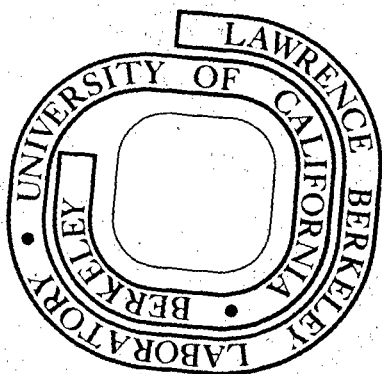
JUN 28 1979

LIBRARY AND  
DOCUMENTS SECTION

Prepared for the U. S. Department of Energy  
under Contract W-7405-ENG-48

TWO-WEEK LOAN COPY

This is a Library Circulating Copy  
which may be borrowed for two weeks.  
For a personal retention copy, call  
Tech. Info. Division, Ext. 6782



LBL-8508 C.2

## **DISCLAIMER**

This document was prepared as an account of work sponsored by the United States Government. While this document is believed to contain correct information, neither the United States Government nor any agency thereof, nor the Regents of the University of California, nor any of their employees, makes any warranty, express or implied, or assumes any legal responsibility for the accuracy, completeness, or usefulness of any information, apparatus, product, or process disclosed, or represents that its use would not infringe privately owned rights. Reference herein to any specific commercial product, process, or service by its trade name, trademark, manufacturer, or otherwise, does not necessarily constitute or imply its endorsement, recommendation, or favoring by the United States Government or any agency thereof, or the Regents of the University of California. The views and opinions of authors expressed herein do not necessarily state or reflect those of the United States Government or any agency thereof or the Regents of the University of California.

A Model for the Anodic Dissolution of Iron in Sulfuric Acid

Clarence G. Law, Jr. and John Newman

Materials and Molecular Research Division, Lawrence Berkeley Laboratory  
and Department of Chemical Engineering, University of California,  
Berkeley, California 94720

May 1979

Abstract

Potential and current distributions are calculated for a partially passivated rotating disk electrode. A discontinuous local polarization relation is used to reflect the change from the active to the passive state. Results of the model yield a z-shaped polarization curve similar to curves measured experimentally by Epelboin et al. The limiting cases of mass transfer control and ohmic control are treated. Comparison of previous experimental results with the model is in harmony with the conclusion that the electrode is mass transfer controlled in the transition region.

### Introduction

Passivation of iron in sulfuric acid has been noticed by investigators for some time. In his experiments Flade<sup>1</sup> observed a potential characteristic of the passive-active state transition. Somewhat later, Osterwald<sup>2</sup> considered the potentiostatic measurements of Franck<sup>3</sup>. An explanation was presented which relates the oscillating current-potential behavior to an ohmic drop in the solution and the stability of an iron oxide film. In a series of papers, Hurlen<sup>4-6</sup> presented kinetic parameters important for the description of the iron electrode. In this paper a model is developed which corresponds to the experimental results obtained with an iron rotating disk electrode in sulfuric acid solution.

More recently, Epelboin et al.<sup>7</sup> showed the importance and validity of an electronic device for obtaining polarization curves. Briefly, they explained the hysteresis of the current-potential curve observed with potentiostatic control in terms of the operating characteristic of the potentiostat. They also introduced a negative impedance converter (N.I.C.). This device was used to control the current-potential behavior of the iron electrode without hysteresis but with a continuous, reversible transition from the active to the passive state. Because of its shape, the curve is referred to as a z shaped curve.

In this paper the portion of the polarization curve which descends from the limiting current plateau to a very small current is called

the transition region. In the transition region, active and passive states exist on different portions of the disk electrode.

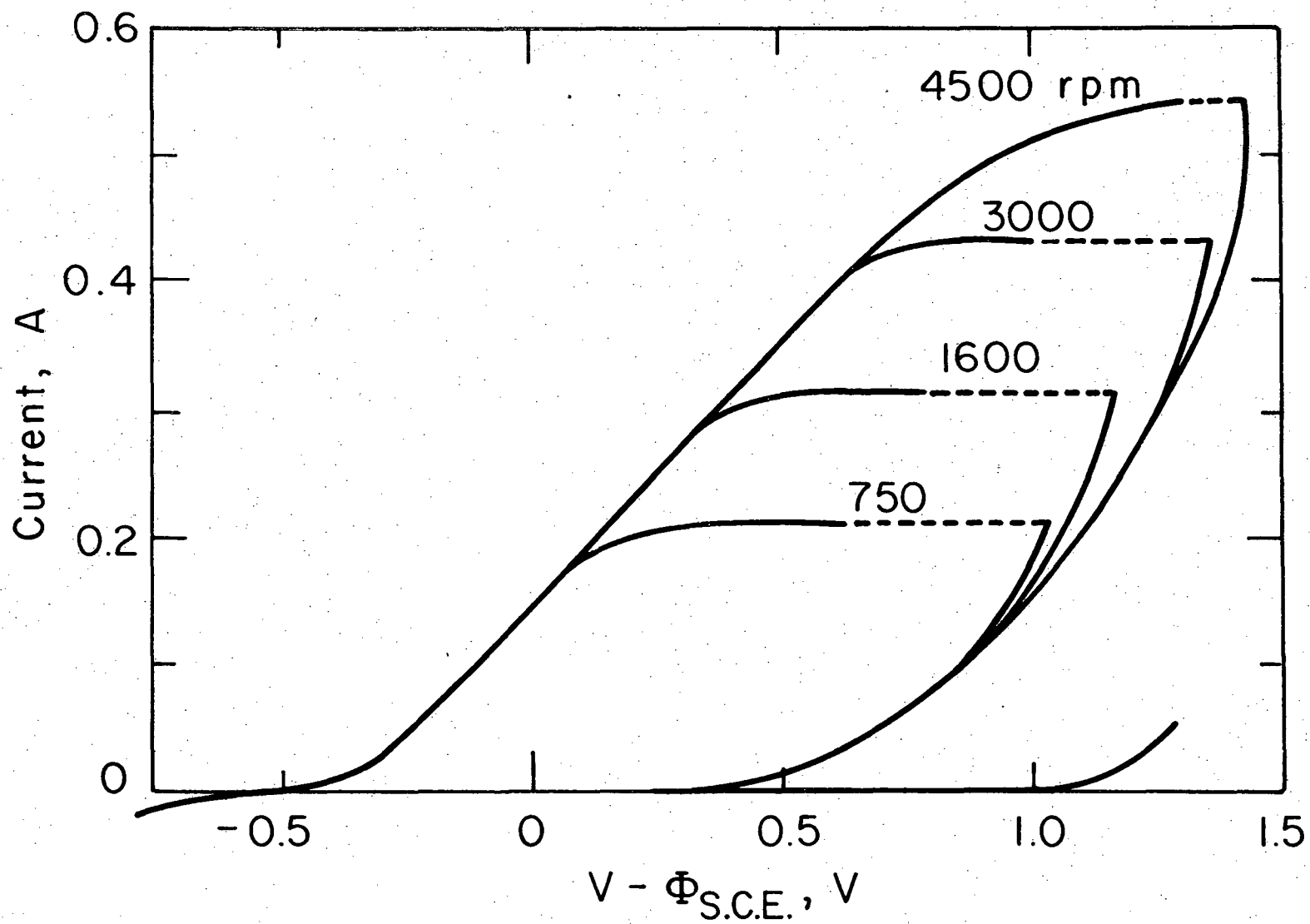
The polarization curves obtained by Epelboin et al. with a N.I.C. are given in figure 1. The limiting current varies with the square root of rotation speed. The dotted region of the plateau is not a stable region; here the measured currents were reported to have large fluctuations.

In their paper Epelboin et al. suggest the applicability of a local polarization relation which decreases sharply to a low current density.

#### Model Development

A simple model is presented for the passivation of iron in 1 molar sulfuric acid which accounts for the kinetic resistance in the double layer and the nonuniform ohmic potential across the disk surface. The model does not consider mass transfer of chemical species explicitly. However, the effect of mass transfer limitations is included in the kinetic expression.

To characterize the overall response of a disk electrode undergoing anodic polarization, a local polarization curve is needed. There are many kinetic expressions from which to choose; however, we have considered an expression which shows a discontinuous change from the active to the passive state. For example, in the active region a modified Butler-Volmer relationship is presumed to apply.



XBL 7812-6335

Figure 1. Current-voltage behavior of a rotating disk electrode obtained by Epelboin et al.

$$i = nFk_a \exp \left[ \frac{\alpha_a F}{RT} (V - \phi_o) \right] - nFk_c c_{Fe^{++}} \exp \left[ \frac{-\alpha_c F}{RT} (V - \phi_o) \right] \quad (1)$$

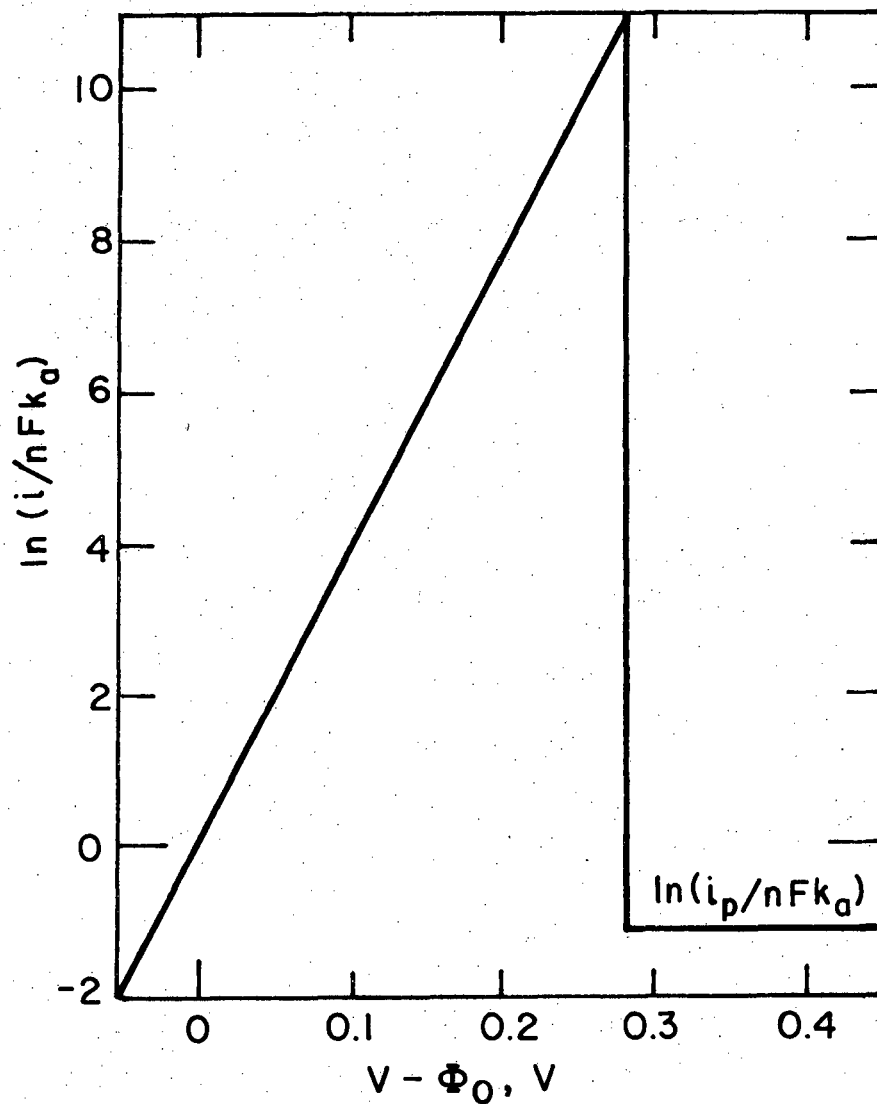
At a characteristic value of the driving force,  $V - \phi_o = (V - \phi_o)_* = 0.28 V$ , a passive film is presumed to form; and the current density changes discontinuously to an extremely low value that remains constant with further increases in  $V - \phi_o$ .

The electric driving force is the local potential difference  $V - \phi_o$ , where  $V$  is the potential of the iron rotating disk electrode and  $\phi_o$  is the potential measured by a saturated calomel electrode immediately adjacent to the surface but outside the double layer. The state of the electrode can be characterized by the value of  $V - \phi_o$ . If  $V - \phi_o$  at the edge is equal to or less than  $(V - \phi_o)_* = 0.28 V$ , then the active state prevails. The passive state exists over the entire disk when  $V - \phi_o$  at the center of the disk is greater than  $(V - \phi_o)_*$ . In the transition region which exists between these conditions, both states exist simultaneously on the disk. Figure 2 is a description of the local polarization relationship.

It is possible to include the effects of mass transfer limitations without explicitly calculating the mass transfer of chemical species. This is accomplished by including the concentration dependence of the limiting reactant in the kinetic expression. An applicable expression is

$$i = nFk_a \left( \frac{c_{R,o}}{c_{R,\infty}} \right)^p \exp \left[ \frac{\alpha_a F}{RT} (V - \phi_o) \right] - nFk_c c_{Fe^{++}} \exp \left[ \frac{-\alpha_c F}{RT} (V - \phi_o) \right] \quad (2)$$





XBL 7812-6336

Figure 2. Local polarization behavior for kinetic control.

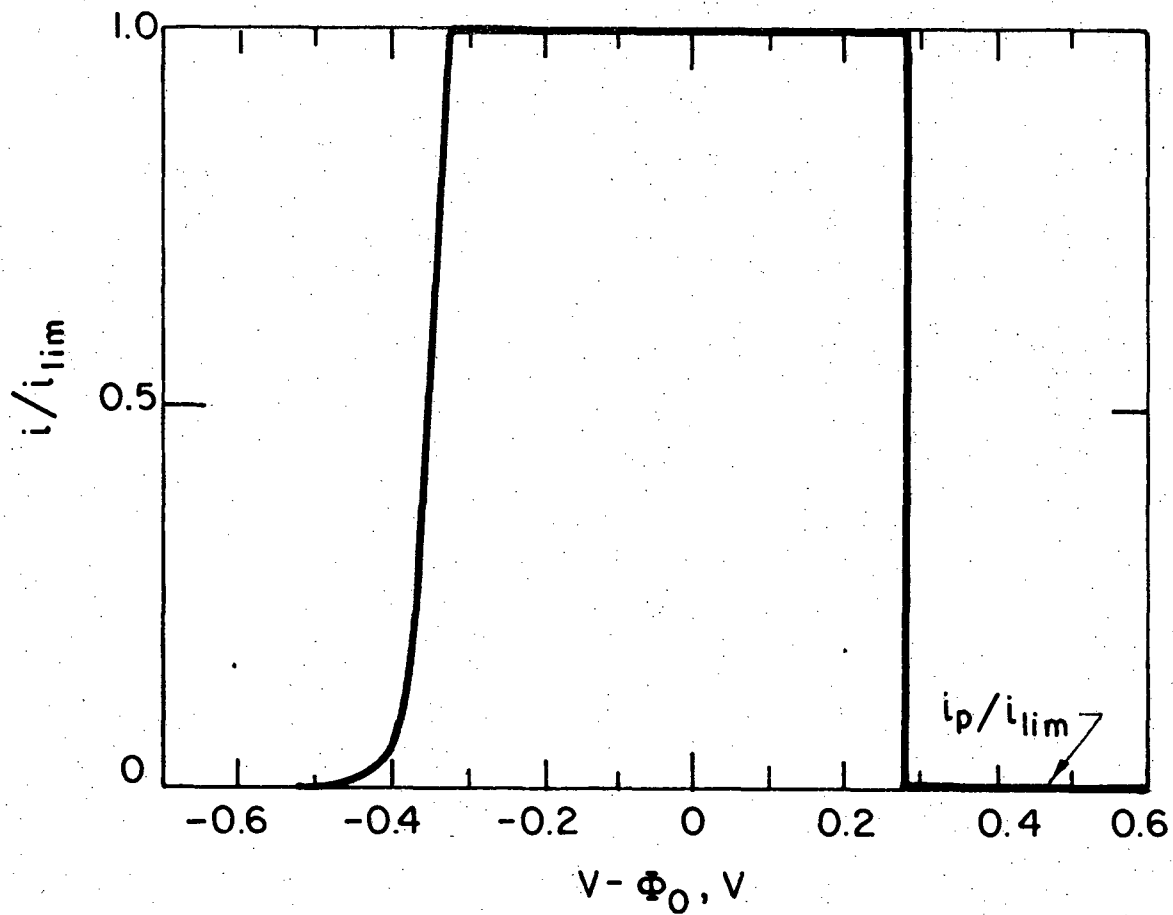
The ratio  $c_{R,0}/c_{R,\infty}$  is equivalent to  $1 - i/i_{lim}$ . The electrode is still presumed to passivate locally for values of  $V - \Phi_0$  greater than  $(V - \Phi_0)_*$ . However, the shape of the local polarization curve is noticeably different. Figure 3 schematically illustrates the local polarization curve when the effect of a limiting species is included. Results will be presented which indicate the merits of the two polarization relations discussed here.

We must mention that the model presented here considers only one of the possible arrangements of the active and passive state. In addition to an active disk with a passive ring outside it, one could also consider a passive disk with an outer active ring, and an active ring between an inner passive disk and an outer passive ring. All three possibilities were observed experimentally by Epelboin et al.

#### Analysis

Laplace's equation is solved for the region between the electrode surface and a counterelectrode well removed from the surface. The equations describing the problem are:

$$\nabla^2 \Phi = 0 \quad (3)$$



XBL7812-6337

Figure 3. Local polarization behavior when mass transfer limitations are considered. While this curve qualitatively represents the behavior for a range of parameters, the curve was actually drawn with  $nFk_a = 1.0 \times 10^6 \text{ A/cm}^2$ ,  $p = 0.01$ , and  $\Omega = 4500 \text{ rpm}$ .

$$\begin{array}{rcl}
 & r = 0 & \phi \text{ is well behaved} & (4) \\
 z = 0 & \left\{ \begin{array}{l} r < r_p \\ r = r_p \\ r_o \geq r > r_p \\ r > r_o \end{array} \right. & \begin{array}{l} i = f(V - \phi_o) \\ V - \phi_o = (V - \phi_o)_* \\ i = i_p = 10^{-4} \text{ A/cm}^2 \\ \frac{\partial \phi}{\partial z} = 0 \end{array} & \begin{array}{l} (5) \\ (6) \\ (7) \\ (8) \end{array} \\
 & z \rightarrow \infty & \phi \rightarrow 0 & (9)
 \end{array}$$

where  $i = f(V - \phi_o)$  refers to equation 1 without mass transfer limitations and to equation 2 when mass transfer limitations are considered.

One does not hope to find a solution to Laplace's equation subject to these boundary conditions in the literature. A solution is obtained by superimposing solutions to Laplace's equation subject to boundary conditions which are algebraically equivalent to those given above. The three solutions are:

$$\phi = \phi^I + \phi^{II} - \phi^{III} \quad (10)$$

where  $\phi^I$ ,  $\phi^{II}$ , and  $\phi^{III}$  all satisfy equations 3, 4, 8, and 9; while on the disk electrode at  $z = 0$ , they satisfy the following

$$r \leq r_p : i^I = f(V - \phi_o), i^{II} = i_p, i^{III} = i_p \quad (11)$$

$$r > r_p : i^I = 0, i^{II} = i_p, i^{III} = 0. \quad (12)$$

A solution for  $\phi^I$  subject to the boundary conditions specified has been given in rotational elliptic coordinates by Newman<sup>8</sup> and takes the form

$$\Phi = \sum_{n=0}^{\infty} B_n P_{2n}(\eta) M_{2n}(\xi) \quad (13)$$

where

$$r = r_p \sqrt{(1 - \eta^2)(1 + \xi^2)}, \quad z = r_p \eta \xi.$$

The current density at the working electrode is given by

$$i = -\kappa \left. \frac{\partial \Phi}{\partial z} \right|_{z=0}. \quad (14)$$

From the orthogonal properties of Legendre polynomials, the  $B_n$  coefficients can be expressed as

$$B_n = \frac{(4n + 1)r_p}{M'_{2n}(0)\kappa} \int_0^1 i(\eta) \eta P_{2n}(\eta) d\eta. \quad (15)$$

It is convenient to use the results of Nanis and Kesselman<sup>9</sup> for solutions to the second and third terms in equation 10. The potential just outside the double layer is the potential of most concern and is given as

$$\Phi_o^{II} = \frac{2}{\pi} \left( \frac{i_p r_o}{\kappa} \right) E \left[ \left( \frac{r}{r_o} \right)^2 \right] \quad r < r_o \quad (16)$$

$$\Phi_o^{II} = \frac{2}{\pi} \left( \frac{i_p r_o}{\kappa} \right) \frac{r}{r_o} \left\{ E \left[ \left( \frac{r_o}{r} \right)^2 \right] - \left[ 1 - \left( \frac{r_o}{r} \right)^2 \right] \left[ K \left( \frac{r_o}{r} \right)^2 \right] \right\} \quad r > r_o. \quad (17)$$

where  $K \left[ \left( \frac{r_o}{r} \right)^2 \right]$  and  $E \left[ \left( \frac{r_o}{r} \right)^2 \right]$  are respectively the complete elliptic

integrals of the first and second kind as defined by Abramowitz and Stegun.<sup>10</sup> (Newman<sup>11</sup> quoted the results of Nanis and Kesselman without realizing the difference in the definition of the elliptic integrals.) A similar expression applies for  $\Phi^{III}$  but with  $r_o$  replaced by  $r_p$ .

### Solution Technique

The current and potential distributions on the active portion of the disk are determined from the  $B_n$  coefficients given by equation 15. To calculate the  $B_n$  coefficients, the  $n$  coupled equations are solved using a multidimensional Newton-Raphson iteration procedure.

To obtain a satisfactory initial guess for the most important  $B$  coefficient,  $B_o$ , this coefficient was made equivalent to the ohmic potential given by the primary resistance relationship for a disk electrode.<sup>12</sup> Thus we set  $B_o = \pi r_p i_{lim} / 4\kappa$ .

In the transition from active to passive state, the point of passivation,  $r_p$ , is unknown. However, a constraint in addition to the  $n$  orthogonal constraints for  $B_n$  is obtained. The value of  $V - \Phi_o$  is specified at the edge of the active region. Computationally it is convenient to replace the unknown  $r_p$  with  $V$ . Therefore the point of passivation is presumed to occur at a specified location, and the potential,  $V$ , of the working disk electrode is calculated. Now the  $n + 1$  equations are calculated using the same Newton-Raphson technique.

In the completely passive region, no detailed calculations are needed as the current density is uniformly equal to  $i_p$ . The potential distribution is simply given by equations 16 and 17.

The Newton-Raphson method was found to be efficient, as convergence was obtained within a few iterations. For the transition region, calculations were also done using a method of successive approximations. Excellent agreement was obtained. However, convergence was very slow for this method, and it was necessary to damp the calculations strongly.

### Results and Discussion

The principal value of the model and the analysis is an overall description of the total current from the rotating iron electrode during anodic polarization. The kinetic parameters used to fit the model to the experimental results are included in Table 1. The solution conductivity from the literature is also given. To obtain an adequate comparison of the experimental results and the model, it is necessary to decide exactly how the comparison should be made. For example, different results and different values of  $k_a$  are used if one decides to match the experimental and calculated currents at the point of passivation versus a good comparison of the kinetically controlled regime.

#### Kinetic considerations

Figure 4 presents a comparison of the experimental results of Epelboin et al. at a rotation speed of 4500 rpm and the model when

Table 1

$$\alpha_a = 1.0 \quad \alpha_c = 1.0 \quad n = 2.0$$

$$nFk_a^\dagger = 1.00 \times 10^7 \text{ A/cm}^2, \quad c_{\text{Fe}^{++}} \quad nFk_c = 8.32 \times 10^{-16} \text{ A/cm}^2$$

$$(V - \Phi_o)_* = 0.28 \text{ V}$$

$$i_p = 1.0 \times 10^{-4} \text{ A/cm}^2$$

$$\kappa = 0.40 \text{ (ohm - cm)}^{-1}$$

$$c_{\text{Fe}^{++}} = 4.0 \text{ mole/litre}$$

$$\beta = 0.17496 \frac{\text{A - sec}^{1/2}}{\text{cm}^2}$$

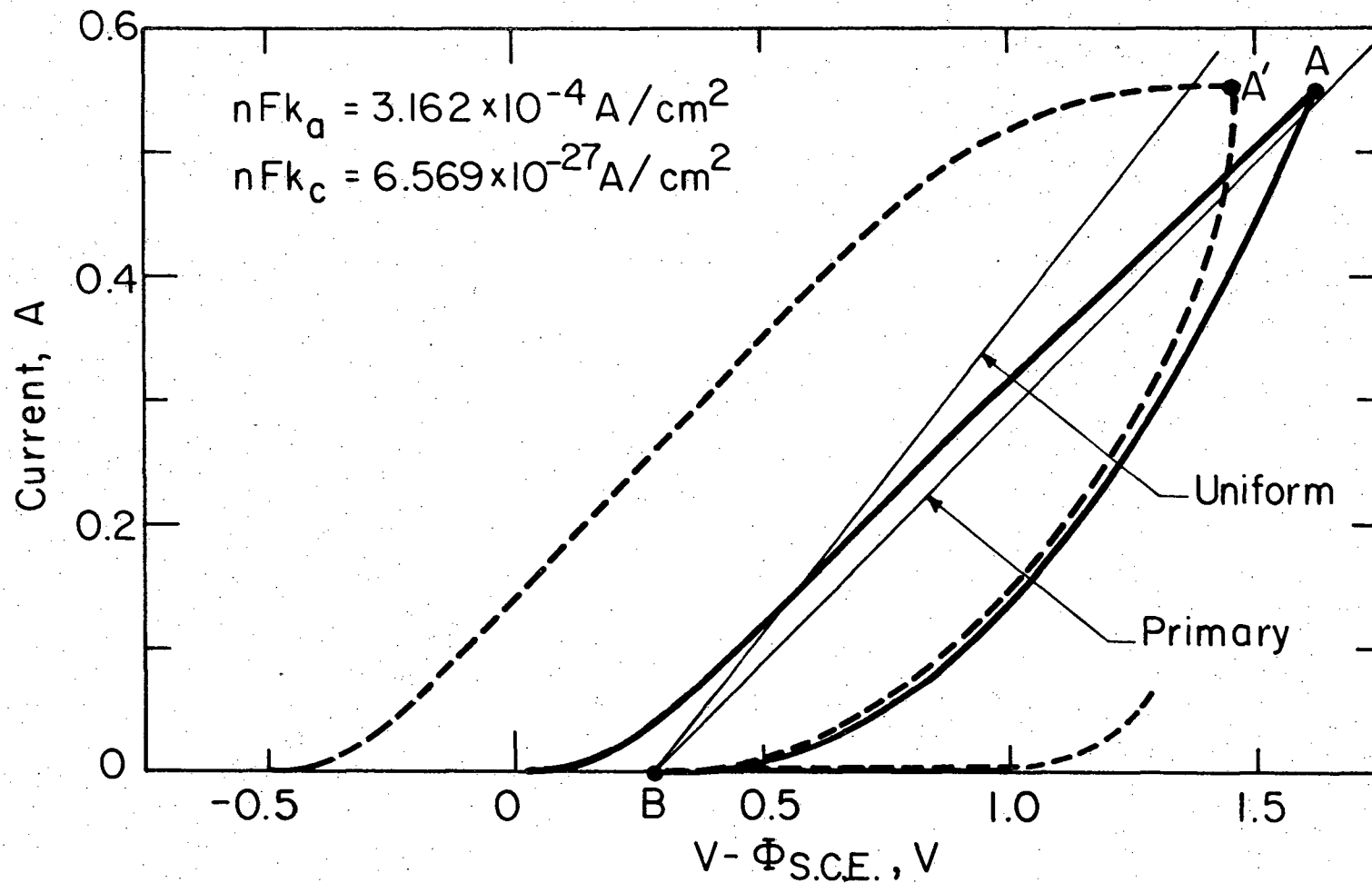
The reference electrode is positioned in the bulk solution.<sup>††</sup>

---

<sup>†</sup>This value of  $k_a$  corresponds to an exchange current density of  $9.1 \times 10^{-5} \text{ A/cm}^2$  at  $c_{\text{Fe}^{++}} = 4.0 \text{ mole/litre}$

<sup>††</sup>Claude Gabrielli, personal communication.





XBL 7812-6338

Figure 4. Comparison of experimental results and calculations when kinetic factors control: (solid line) calculations, (dashed line) experimental results. The lines marked uniform and primary refer to the transition region behavior of a completely active disk which passivates at  $(V - \Phi_0)_* = 0.28 \text{ V}$  at its edge for the respective current density distributions

the value of  $k_a$  is such that  $I_{\text{calc}} = I_{\text{expr}}$  at the point where the disk begins to passivate. The highest rotation speed was chosen since mass transfer limitations were less than at the lower speeds. A good agreement in the transition region is obtained at the expense of poor agreement in the active kinetic region.

The transition region shown in figure 4 does not normally occur for an active electrode. Normally increases in  $V - \phi_{\text{ref}}$  result in further increases in  $I$ . However, from the viewpoint of the model, the transition region occurs as a result of boundary condition 6 and the ohmic potential drop. As one travels along the transition region from A to B, the size of the active portion decreases, and the total disk current drops. To see how the electrode potential varies in this region it is helpful to recall the simple relationship for the primary resistance for a disk electrode given by Newman.<sup>12</sup>

$$\frac{\phi_o}{I} = \frac{1}{4\kappa r_o} \quad (18)$$

Since  $V - \phi_o$  is specified at  $r = r_p$ , the value of  $V - \phi_{\text{ref}}$  approaches 0.28 V as  $I$  and  $r_p$  approach zero. However, since  $r_o$  should here be replaced by  $r_p$  in equation 18, the decreasing part of the transition is not linear but is bowed outward as shown in figure 4.

The shape of the transition can be seen in view of the current density specified at the edge and equation 18. The measured driving force can be written as

$$V - \Phi_{\text{ref}} = V - \Phi_o(r = r_p) + (\Phi_o(r = r_p) - \Phi_{\text{ref}}) \quad (19)$$

or alternatively

$$V - \Phi_{\text{ref}} = 0.28 + \Phi_o(r = r_p) - \Phi_{\text{ref}} \quad (20)$$

It is convenient to express  $\Phi_o(r = r_p)$  as

$$\Phi_o(r = r_p) = \frac{\epsilon I}{4\kappa r_p} \quad (21)$$

where  $\epsilon$  is a number which varies from 1 for a primary distribution to  $\frac{8}{\pi^2} = 0.810569$  for a uniform distribution. Since  $r_p$  is unknown, let us replace it with the average current density  $i_{\text{avg}}$  according to

$$I = \pi r_p^2 i_{\text{avg}}$$

(with neglect of the small current on the passivated part of the disk).

The electrode polarization in the transition region can now be expressed as

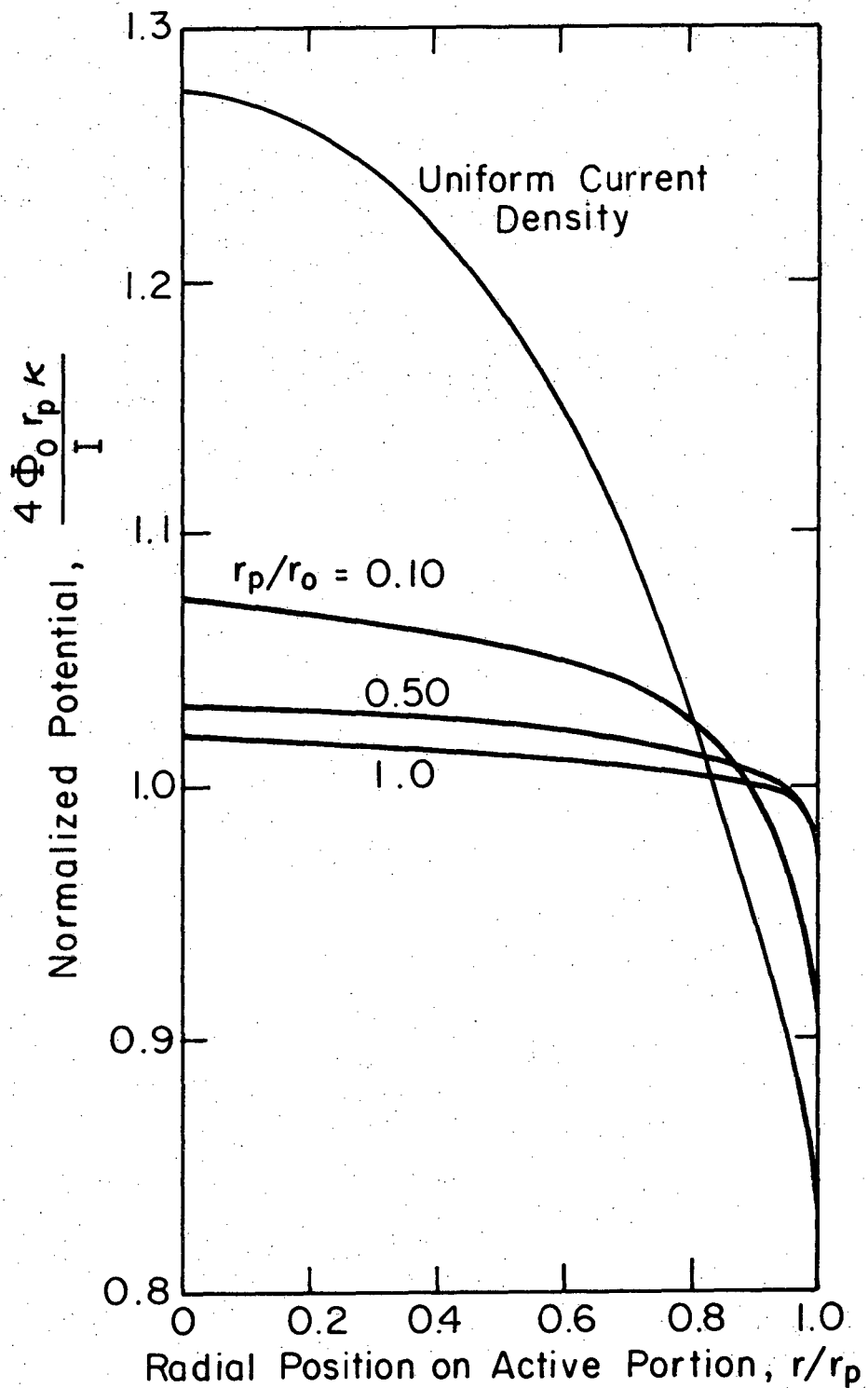
$$V - \Phi_{\text{ref}} = 0.28 + \frac{\epsilon \sqrt{\pi I i_{\text{avg}}}}{4\kappa} - \Phi_{\text{ref}} \quad (22)$$

In the experimental system, the reference electrode is in the bulk solution, and  $\Phi_{\text{ref}}$  is essentially zero. Then, this relationship shows that the calculated transition region curve should be a parabola if the average current density on the active portion and  $\epsilon$  remain constant. The experimental curves have approximately this shape, and deviations can be explained in terms of variations in  $i_{\text{avg}}$  and  $\epsilon$ .

Returning to figure 4, we observe that both the experimental and calculated curves deviate from a parabolic shape over the range of the transition. If point A' represents an entirely active electrode, then the difference between A and A' is attributable to different current distributions. Point A' has a more uniform distribution than that at the calculated point A.

Near point B the calculated results approach a disk of uniform current density, since the current density approaches that given by equation 6. Using equation 22 we can determine that the current density at the bottom is greater than at the top of curve B-A. One can also conclude that the distortion from a parabola is caused by an increase in  $i_{avg}$  from A' to B in addition to changes in  $\epsilon$ .

To show the calculated variation in current distribution that occurs over the course of the transition region, figure 5 is presented. Following Newman,<sup>13</sup> we have normalized the ohmic potential with respect to the primary resistance for a disk of radius  $r_p$ . The uniform current density limit is provided for reference. One notices that as the active surface area decreases the current density on the active portion becomes more nearly uniform. For example, the ratio of the current density at the center to that at the edge varies from 0.07 when  $r_p/r_o = 1.0$  to 1 when  $r_p/r_o = 0$ . The current distribution approaches the uniform limit as  $r_p/r_o \rightarrow 0$  and the primary limit when  $r_p = r_o$ .



XBL7812-6339

Figure 5. Variation of the ohmic potential across the active portion of the disk.

### Mass transfer limitations

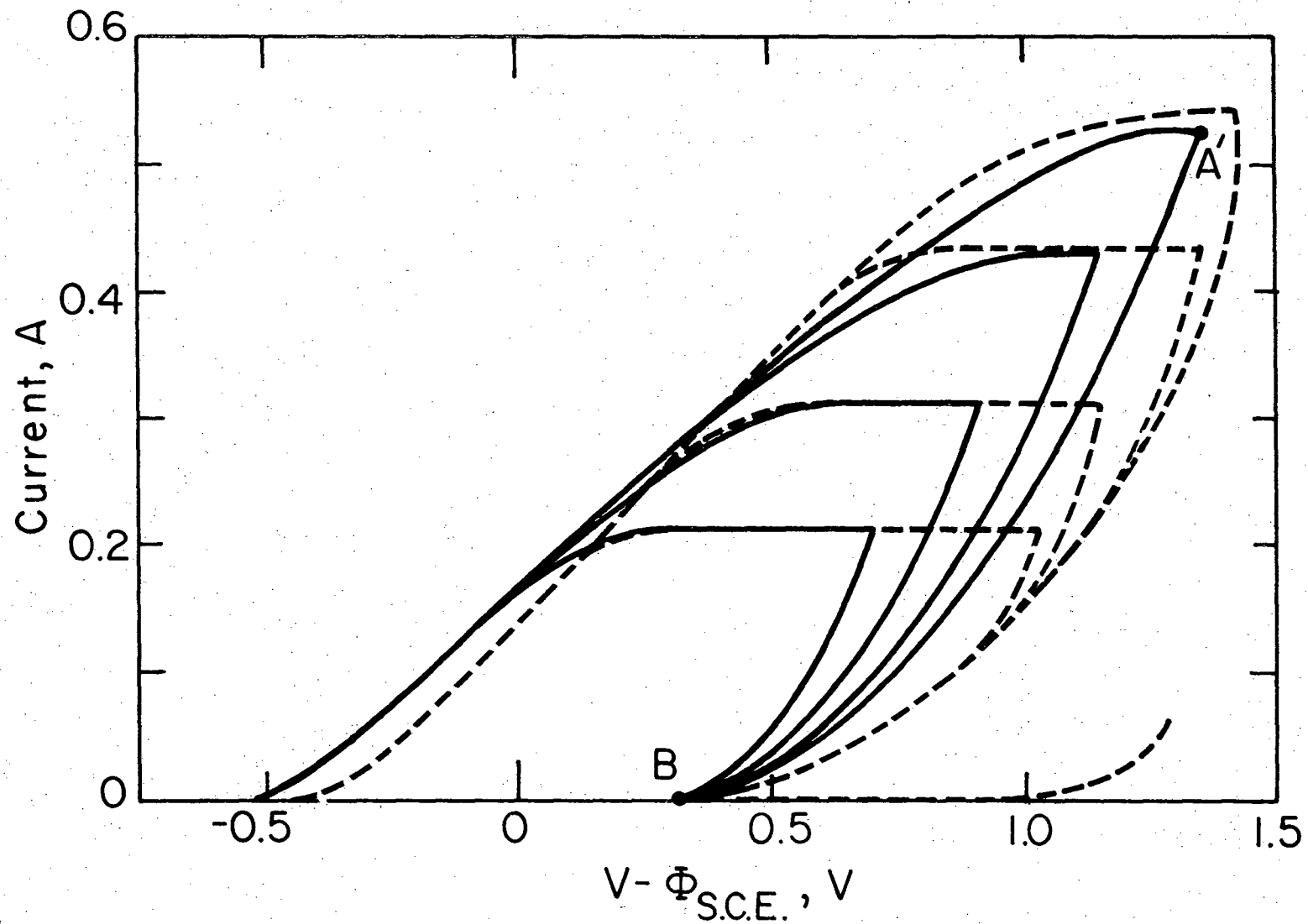
If one considers mass transfer limitations, a local polarization relation given by equation 2 is valid. The results of the model using this equation are given in figure 6. Parameters are again given in Table 1.  $\beta$  is determined from the data and the defining relation

$$i_{lim} = \beta\sqrt{\Omega} . \quad (23)$$

It is also necessary to specify the reaction order,  $p$ , of the limiting reactant. Levich<sup>15</sup> has indicated the effect of the reaction order on the approach to a limiting current plateau; for smaller values of  $p$  the curve follows more closely the kinetic and limiting-current limits. Figure 7 shows the effects of varying the reaction order  $p$  of the limiting reactant.

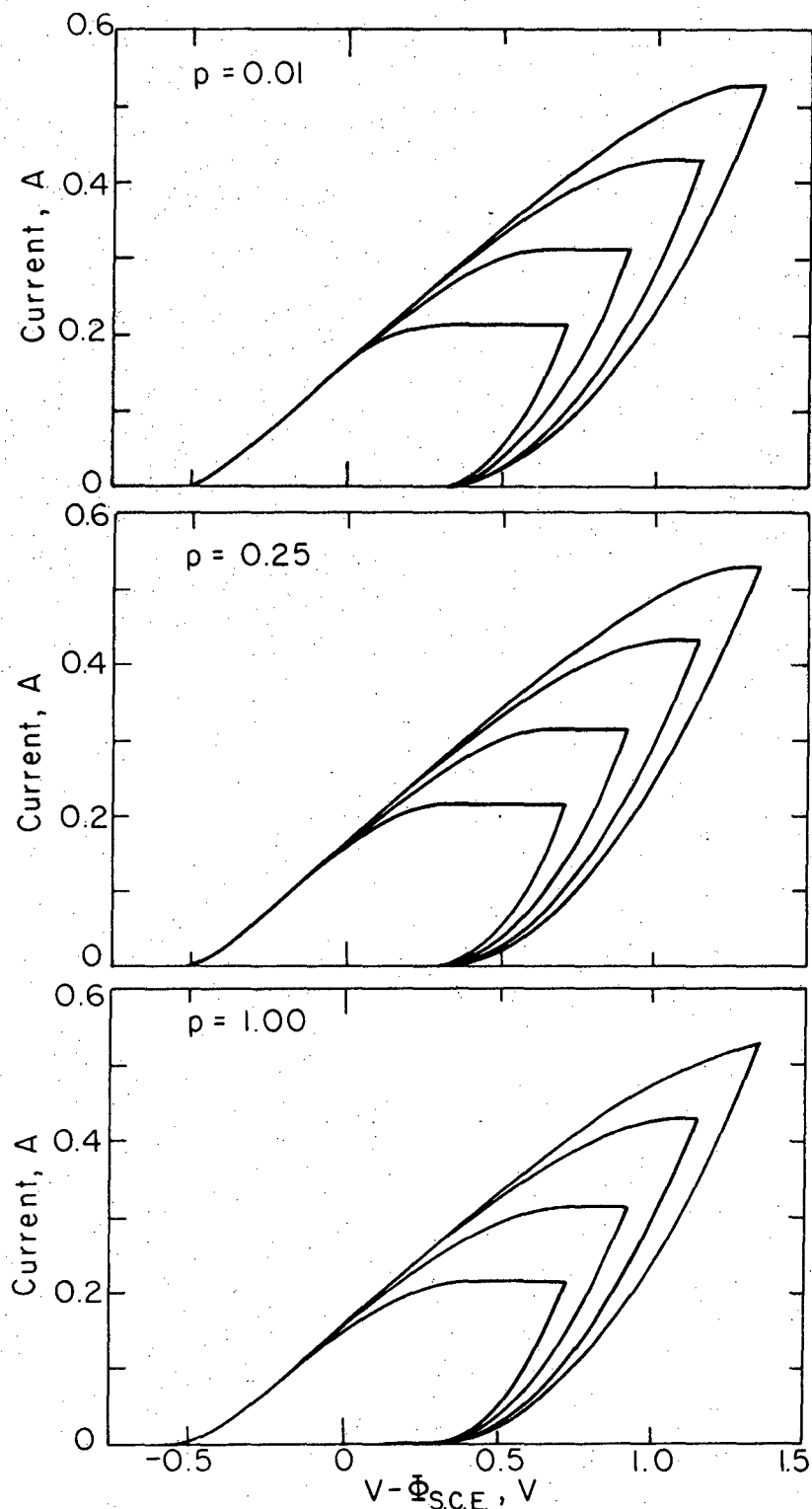
The calculated transition region shown in figures 6 and 7 is substantially mass transfer controlled. As one proceeds from the completely active to the completely passive state, the current density is uniform across the disk and given by equation 23. The decrease in current is completely attributable to the decrease of the active area.

A discrepancy between the model and the experiments is revealed in figure 6. The model yields four distinct curves in the transition which are characteristic of the four rotation speeds. In the lower portion of the transition, the experimental curves overlap. The four distinct curves of the model indicate four different average or limiting current densities, although the superimposed experimental curves give evidence of the same uniform current density existing for



XBL 7812-6340

Figure 6. Comparison of measured and calculated polarization curves: (solid line) calculations ( $p = 0.01$ ), (dashed line) experimental results--(reference 7).



XBL7812-6341A

Figure 7. Comparison of calculated polarization curves for different reaction orders of the limiting reactant. The four curves for any given value of  $p$  correspond to rotation speeds of 750, 1600, 3000, and 4500 rpm.

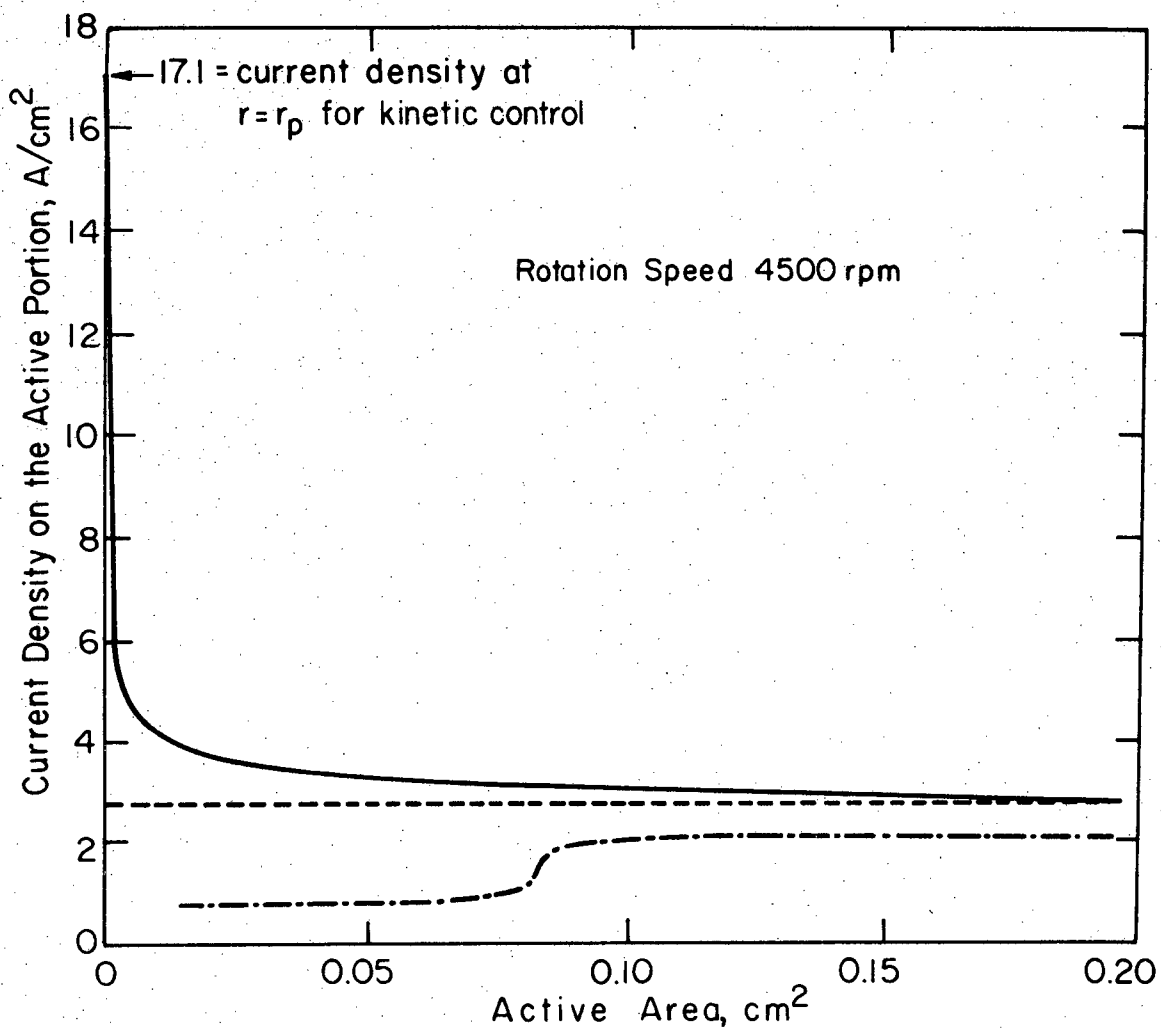


all four rotation speeds. The experimental curves also reflect an increase in the average current density as one travels toward the passive state.

Epelboin et al. made measurements of the total current from the disk electrode and the dimensions of the active electrode. Figure 8 presents the results of these measurements and calculations from the model. However, it should be emphasized that some of the experimental results indicated that the current was restricted to a thin ring and no noticeable faradaic reaction occurred inside the inner radius or beyond the outer radius of the ring, whereas the model considers an active disk whose radius decreases as the passive state is approached. Therefore, comparison of the model with the experimental results for equivalent areas may compare the results of rings with those of a disk.

The upper curve on figure 8 refers to the situation where kinetic factors determine the current distribution on the disk (as was the case for the calculations shown in figure 4). Here the average current density on the disk in the transition region increases markedly as the size of the active disk approaches zero, although the increase is gradual for relatively large values of the active area.

The horizontal line on figure 8 is characteristic of a mass transfer controlled active-disk region (as was the case for calculations shown in figures 6 and 7). The experimental results of Epelboin et al. appear to resemble closely the behavior typical of a mass transfer region. In fact, their results look like two mass transfer regions coupled by a steep transition. Most of their experimental curve is



XBL 7812-6342

Figure 8. Current density on the active portion of the disk electrode in the transition region: (—•) experimental results of Epelboin et al., (dashed line) results of the model when mass transfer effects are included, (solid line) results of the kinetic model.

for ring shapes. It is remarkable that a mass transfer controlled ring region would have a lower average current density than a disk region. One is also surprised that the experimental curve and the horizontal line do not meet when the disk is completely active as this shows an inconsistency between  $i_{avg}$  obtained from  $\beta\sqrt{\Omega}$  and  $i_{avg}$  obtained from  $I$  and measurements of the active dimensions. An explanation could be given in terms of a region existing near  $A'$  (figure 6) where the disk remains active and a decrease in the current density occurs. Of course, the model presented here cannot substantiate this.

#### Consideration of ring shapes

Since a significant portion of the transition region is a ring and not a disk, one should consider whether a consideration of rings can account for the average current density decreasing as the passive state is approached (figure 8). A comparison of the measured potential and current with that calculated for rings may clarify this matter. Consider a normalized resistance function,  $g(r_i/r_p)$ , which contains the important measured parameters.

$$g(r_i/r_p) = \frac{\kappa\Phi_o(r = r_p)}{\sqrt{i_{lim}} \sqrt{I}} \quad (24)$$

where

$$\Phi_o(r = r_p) = V - \Phi_{ref} - 0.28 .$$

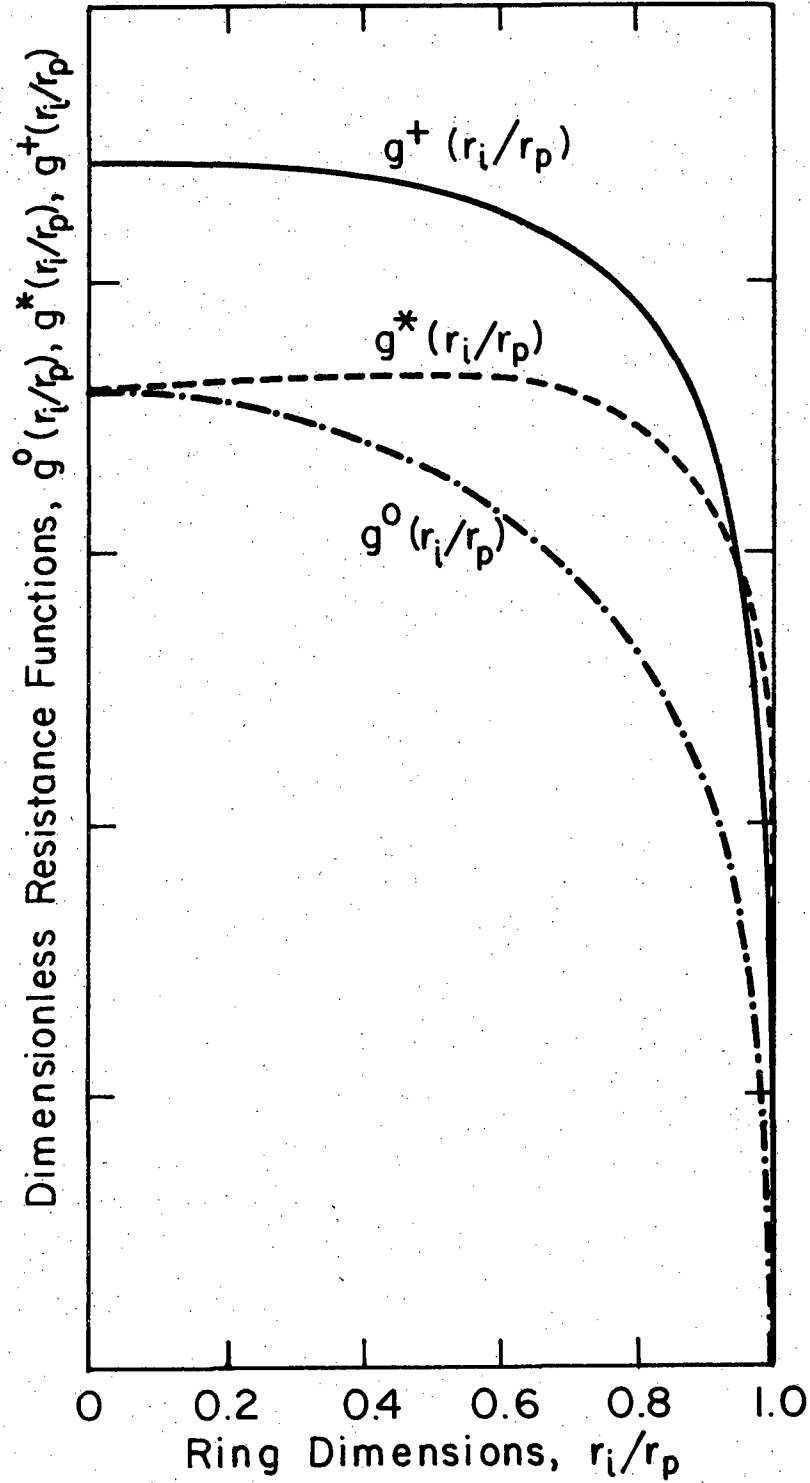
Therefore with choice of a rotation speed, measured potential, and current, a value of  $g(r_i/r_p)$  is defined. This measured value of  $g$  can be compared with functions defined for rings of various current distributions. Namely, consider  $g^0$  defined by a ring of uniform current,  $i_{avg} = \beta\sqrt{\Omega}$ ;  $g^*$  defined by a ring of average current density,  $i_{avg} = \beta\sqrt{\Omega} f(r)$  and the primary resistance of a ring given by

Miksis and Newman.<sup>16</sup>  $f(r)$  is defined by Newman<sup>17</sup> as 
$$\frac{\left[1 - \left(\frac{r_i}{r_p}\right)^3\right]^{2/3}}{\left[1 - \left(\frac{r_i}{r_p}\right)^2\right]}$$

$\Phi_0(r = r_p)$  for  $g^0$  and  $g^*$  are calculated using the results of Nanis and Kesselman.  $g^*$  can be related to  $g^0$  by

$$g^*(r_i/r_p) = g^0(r_i/r_p) \sqrt{f(r)}. \quad (25)$$

Figure 9 illustrates the behavior of these functions. It is important to compare values of  $g$  obtained experimentally with  $g^0$ ,  $g^*$ , and  $g^+$ . For example, if we consider a point where  $\Omega$  4500 rpm,  $I = 0.54$  A,  $i_{lim} = 2.80$  A/cm<sup>2</sup>,  $V - \Phi_{ref} = 1.42$  V, then  $g(r_i/r_p)$  is calculated to be 0.37. This is the smallest value of  $g$  one can obtain from the data. For this example  $g$  intersects the  $g^+$  curve,  $r_i/r_p = 0.85$ , which corresponds to a thin ring near the periphery of the disk. However, it is inconsistent to have a  $g$  value obtained near the limiting current plateau equivalent to a calculated value of  $g$ ,  $g^+$ , which corresponds to the primary resistance of a thin ring. An increase



XBL 7812-6343

Figure 9. Correlation of normalized resistance functions.

in  $i_{lim}$  will lower the value of  $g$  and it will approach the more appropriate values of  $g^o$  and  $g^*$ . Also, as one travels down the transition region, the current distribution becomes more uniform and increases in  $i_{avg}$  must occur.

### Summary and Conclusions

The simple model presented yields a z-shaped curve for the anodic polarization of iron in sulfuric acid very similar to that obtained experimentally by Epelboin et al. The model accounts for the kinetic resistance at the surface, the ohmic potential, and the effect of mass transfer limitations. In the transition region the model predicts the same general response of the disk electrode for the limit of mass transfer control and for the case of kinetic control. However, the calculated current density remains constant in the transition region when mass transfer limitations are included, whereas the current density increases in the transition region as the passive state is approached when strictly kinetic factors are considered. Epelboin et al. report current densities which decrease in the transition. Analysis presented here states that the experimentally obtained average current density must increase as the passive state is obtained. The analysis is valid for both disk and ring shapes.

### Acknowledgement

This work was supported by the Division of Chemical Sciences, Office of Basic Energy Sciences, U.S. Department of Energy under contract No. W-7405-Eng-48.

Notation

$B_n$	coefficient in the expansion for the potential, V
$c_{Fe^{++}}$	concentration of ferrous ions at the electrode surface, mole/litre
$c_{R,o}$	concentration of the limiting reactant at the electrode surface, mole/litre
$c_{R,\infty}$	concentration of the limiting reactant in the bulk solution, mole/litre
E	complete elliptic integral of the second kind
F	Faraday's constant, 96,487 C/mol
f	dimensionless ratio defined in reference 17
g	normalized resistance, defined by equation 24
$g^o$	normalized resistance, figure 9
$g^*$	normalized resistance, figure 9
$g^+$	normalized resistance, figure 9
i	local current density, A/cm <sup>2</sup>
$i_{avg}$	average current density, A/cm <sup>2</sup>
$i_{lim}$	limiting current density, A/cm <sup>2</sup>
$i_p$	current density on the passive portion of the disk, A/cm <sup>2</sup>
I	total current on the disk, A
K	complete elliptic integral of the first kind
$k_a$	anodic rate constant, mole/sec cm <sup>2</sup>
$k_c$	cathodic rate constant, mole/sec cm <sup>2</sup>
$M_{2n}$	Legendre function of imaginary argument
n	number of electrons transferred
$P_{2n}$	Legendre polynomial of order 2n

p	reaction order of limiting reactant
R	universal gas constant, 8.3143 J/mol -K
r	radial coordinate, cm
$r_i$	inner radius of the ring, cm
$r_o$	electrode radius, cm
$r_p$	radius of the active portion, cm
T	absolute temperature, K
V	potential of rotating disk electrode, V
$(V-\phi_o)_*$	passivation potential, 0.28 V
z	axial coordinate, cm
$\alpha_a$	anodic transfer coefficient
$\alpha_c$	cathodic transfer coefficient
$\beta$	constant in equation , A-sec <sup>1/2</sup> /-cm <sup>2</sup>
$\epsilon$	defined by equation 21
$\eta$	rotational elliptic coordinate
$\kappa$	bulk solution conductivity, ohm <sup>-1</sup> - cm <sup>-1</sup>
$\xi$	rotational elliptic coordinate
$\phi^I, \phi^{II}, \phi^{III}$	potential in the solution, V
$\phi_o$	solution potential immediately adjacent to the electrode surface, V
$\Omega$	rotation speed of the disk



References

1. Fr. Flade, "Beiträge zur Kenntnis der Passivität," Zeitschrift für Physikalische Chemie, 76, 513-559 (1911).
2. Jörg Osterwald, "Die Stromspannungskurve des Eisens in Schwefelsäure beim Übergang vom aktiven in den passiven Zustand," Zeitschrift für Elektrochemie, 66, 401-406 (1962), also UCRL-Trans-1544 (1977).
3. Ulrich F. Franck, "Über das anodische Verhalten des Eisens in Schwefelsäure," Zeitschrift für Naturforschung, 4a, 378-397 (1949).
4. Tor Hurlen, "Electrochemical Behaviour of Iron," Acta Chemica Scandinavica, 14, 1533-1554 (1960).
5. Tor Hurlen, "Corrosion of Iron Effect of pH and Ferrous Ion Activity," Acta Chemica Scandinavica, 14, 1555-1563 (1960).
6. Tor Hurlen, "Heat of Activation in Electrode Kinetics The Fe/Fe<sup>++</sup> aq Electrode," Acta Chemica Scandinavica, 14, 1564-1570 (1960).
7. Israël Epelboin et al., "Passivation of Iron in Sulfuric Acid Medium," Journal of the Electrochemical Society, 119, 1632-1637 (1972).
8. John Newman, "Current Distribution on a Rotating Disk below the Limiting Current," Journal of the Electrochemical Society, 113, 1235-1241 (1966).
9. Leonard Nanis and Wallace Kesselman, "Engineering Applications of Current and Potential Distributions in Disk Electrode Systems," Journal of the Electrochemical Society, 118, 454-461 (1971).

10. Milton Abramowitz and Irene A. Stegun, eds., Handbook of Mathematical Functions, p. 590, National Bureau of Standards, Washington, D.C. (1965).
11. John Newman, "The Fundamental Principles of Current Distribution and Mass Transport in Electrochemical Cells," p. 328, Allen J. Bard, ed., Electroanalytical Chemistry (New York: Marcel Dekker, Inc., 1973), 6, 187-352.
12. John Newman, "Resistance for Flow of Current to a Disk," Journal of the Electrochemical Society, 113, 501-502 (1966).
13. John S. Newman, Electrochemical Systems, p. 350, Englewood Cliffs: Prentice-Hall, Inc., 1973.
14. Thomas W. Chapman and John Newman, "A Compilation of Selected Thermodynamic and Transport Properties of Binary Electrolytes in Aqueous Solution," UCRL-17767, (1968).
15. Veniamin G. Levich, Physiochemical Hydrodynamics, p. 76, Englewood Cliffs: Prentice-Hall, Inc., 1962.
16. Joseph J. Miksis, Jr. and John Newman, "Primary Resistance for Ring-Disk Electrodes," Journal of the Electrochemical Society, 123, 383-385 (1976).
17. John S. Newman, Electrochemical Systems, p. 336, Englewood Cliffs: Prentice-Hall, Inc., 1973.

This report was done with support from the Department of Energy. Any conclusions or opinions expressed in this report represent solely those of the author(s) and not necessarily those of The Regents of the University of California, the Lawrence Berkeley Laboratory or the Department of Energy.

Reference to a company or product name does not imply approval or recommendation of the product by the University of California or the U.S. Department of Energy to the exclusion of others that may be suitable.

TECHNICAL INFORMATION DEPARTMENT  
LAWRENCE BERKELEY LABORATORY  
UNIVERSITY OF CALIFORNIA  
BERKELEY, CALIFORNIA 94720